Hindawi
Mathematical Problems in Engineering
Volume 2019, Article ID 5432470, 13 pages
https://doi.org/10.1155/2019/5432470

Research Article

The Effects of Confining Stress on Rock Fragmentation by TBM Disc Cutters

S. F. Zhai[1,2] **S. H. Cao**[1] **M. Gao**[1] **and Y. Feng**[1]

[1]*College of Civil Engineering and Architecture, Henan University of Technology, Zhengzhou 450000, China*
[2]*Department of Civil Engineering, Chongqing University, Chongqing 400045, China*

Correspondence should be addressed to S. F. Zhai; zhaishufangcqu@126.com

Received 13 September 2018; Accepted 11 October 2018; Published 9 January 2019

Academic Editor: Roberto G. Citarella

In this paper, General Particle Dynamics (GPD3D) is developed to simulate rock fragmentation by TBM disc cutters under different confining stress. The processes of rock fragmentation without confining pressure by one disc cutter and two disc cutters are investigated using GPD3D. The crushed zone, initiation and propagation of cracks, and the chipping of rocks obtained from the proposed method are in good agreement with those obtained from the previous experimental and numerical results. The effects of different confining pressure on rock fragmentation are investigated using GPD3D. It is found that the crack initiation forces significantly increase as the confining stress increases, while the maximum angle of cracks decreases as the confining stress increases. The numerical results obtained from the proposed method agree well with those in previous indentation tests. Moreover, the effects of equivalent confining stress on rock fragmentation are studied using GPD3D, and it is found that rock fragmentation becomes easier when the equivalent confining stress is equal to 15MPa.

1. Introduction

In recent years, tunnel boring machine (TBM) has been extensively used in the underground engineering because of high advance rates and safety performance. During the tunneling process, the TBM machine interacts with rock masses, so the rock mass structure, properties, and geological environment (such as the jointing growth condition, confining stress, and groundwater) have significant impact on the performance of TBM machine. Up to now, many researches have investigated the effects of confining stress on rock fragmentation by TBM disc cutters, and there are two main approaches to study the issue, which are, respectively, laboratory indentation test and numerical simulation.

Experimentally, Gehring [1] found that the cutter consumption under high confining stress is greater than that under lower overburden in the field of TBM tunneling. Huang et al. [2] studied the influence of the lateral confining stress on the development of damaged rock and the initiation of tensile fractures and found that the position of the maximum tensile stress is dramatically deviated from the indentation axis with a small increment in the confining stress. Innaurato et al. [3] found that a slight effect of the lateral confinement on the load may cause the rock breakage, if the cutter spacing is efficient. Yin et al. [4] found from the indentation test that the crack initiation stress and crushed zone size increase, and cracks tend to propagate towards the free surface when the confining stress increases.

In the numerical simulation, Gong et al. [5] introduced discrete element method (DEM) to investigate the rock fragmentation by disc cutters. The results obtained from these numerical simulations are in good agreement with the experimental ones. Based on a micromechanics-based numerical code, Ma et al. [6] studied the rock fragmentation processes under different confinement, and the confining conditions for TBM tunneling are divided into three general classes through an index of the confining ratio defined as the ratio of confining stress to uniaxial compressive strength. On the basis of theoretical investigation and numerical simulation of PFC, Liu et al. [7] found that cutting efficiency increases as the confining stress increases in a certain degree, while the efficiency is restrained by the increasing confining stress as the confining stress exceeds a critical value.

From the above studies, in the past years, several numerical approaches were used to solve the rock fragmentation problems, such as finite element method (FEM) and discrete element method (DEM). However, FEM is limited because the finite element meshes coincide with cracks. This limitation makes the task of generating the mesh very difficult. When cracks propagate during rock fragmentation, remeshing is inevitable, which makes it nearly impossible to model rock fragmentation problems with FEM [8].

DEM serves an important approach to investigate the rock chipping mechanism induced by the TBM cutters. Unfortunately, as mentioned in works by Donze et al. [9], (1) fracture is closely related to the size of elements and that is the so-called size effect, (2) cross effect exists because of the difference between the size and shape of elements with real grains, and (3) in order to establish the relationship between the local and macroscopic constitutive laws, data obtained from classical geomechanical tests which may be impractical are used.

Besides, most numerical studies were conducted on two-dimensional models, which may not be identical to the true physics of rock fragmentation by TBM cutters. In this study, a 3D numerical method known as General Particle Dynamics (GPD3D) [10, 11] is introduced to investigate the rock fragmentation by disc cutter under different confining stress. This mesh-free numerical method overcomes the shortcomings of Smooth Particle Hydrodynamics (SPH) and can determinate the paths of crack growth and fragmentation under loads. In GPD3D, it is assumed that one particle is killed when its stresses satisfy the critical value, and the killed particle has no effect on its neighbors during the deformation process. This is reasonable as the kernel usually distributes larger weightage just around the particle of interest, and the quantity of these immediate particles is enough. During the deformation process, one particle's life is determined based on the accumulated stress and a fully damaged particle is considered as the initiation of crack. In this paper, an elastic brittle damage model based on 3D Hoek-Brown criterion [12] is adopted to simulate the process of rock fragmentation by TBM cutters.

The paper is organized as follows. In Section 2, the strength criterion and damage model for GPD3D is outlined. In Section 3, the processes of rock fragmentation without confining stress by one disc cutter and two disc cutters are investigated using GPD3D. In Section 4, the effectiveness of GPD3D on rock fragmentation by one TBM disc cutter under different confining stress is validated. In Section 5, the effects of equivalent confining stress on rock fragmentation by one TBM disc cutter are investigated using GPD3D. Conclusions are drawn in Section 6.

2. The Strength Criterion and Damage Model for General Particle Dynamics (GPD3D)

In this paper, only the strength criterion and the damage model implemented in the GPD are described in detail because the general formulations of the methods such as constitutive model, governing equations, and correction for consistency have been stated in the previous works [10, 11].

In most cases, rock-like materials fail in a brittle manner. All the particles have the same parameters as those of the parent material (i.e., uniaxial compressive strength, Young's modulus (E), and Poisson ratio (ν)); therefore, the damage initiation and growth in the particles are determined by the damage model of materials. The algorithm is described as follows.

In this paper, the 3D Hoek-Brown criterion is applied to determine damage initiation. Damage is believed to be initiated from one particle when stresses in the particle satisfy the 3D Hoek-Brown criterion. In order to enhance applicability of the 3D Hoek-Brown criterion, there are several correct versions and the latest version is proposed for rocks as follows [13]:

$$\frac{2\left[1+\cos\left(1/3-2\theta\right)\right]}{m_b\sigma_i}J_2' + \frac{2\cos\left(\pi/3-\theta\right)}{\sqrt{3}}\sqrt{J_2'} - \frac{s}{m_b}\sigma_i = \frac{I_3'}{3} \tag{1}$$

where σ_i is a uniaxial compressive strength of an intact rock material, J_2' is the second invariants of the stress deviator, θ is Lode's angle of stress varying from 0 to $\pi/3$, and m_b and s are the material parameters in the Hoek-Brown criterion, which are defined by Hoek et al. and take the following form [14, 15]:

$$m = m_i \exp\left(\frac{GSI-100}{28-14D}\right) \tag{2}$$

$$s = \exp\left(\frac{GSI-100}{9-3D}\right) \tag{3}$$

where D *is* a disturbance coefficient which varies from 0.0 for the undisturbed in situ rock masses to 1.0 for very disturbed rock masses. GSI is short for Geological Strength Index which reflects the fragmentation degree of rock mass and it is equal to 100 for the intact rock, m_i is the value of m for intact rock and can be obtained from experiments, and the parameter m_i varies from 4 for very fine weak rock-like claystone to 33 for coarse igneous light-colored rock-like granite.

Now we introduce a parameter f, coined as the "interaction factor" which defines the level of interaction between the i-th and the j-th particles. The interaction factor f is determined based on the damage in particles. Initially, for undamaged particles, $f = 1$, which implies "full interaction". With progress of damage, f finally becomes zero for fully damaged particle. In order to model the damage growth, a linear elastic brittle law, as shown in Figure 1, is used.

$$\omega = 0, \quad \textit{and } f = 1, \quad (\textit{if } \sigma_i < \sigma_{\max}) \tag{4}$$

$$\omega = 1, \quad \textit{and } f = 0, \quad (\textit{if particle damaged}) \tag{5}$$

where ω is the damage factor and f is the interaction factor.

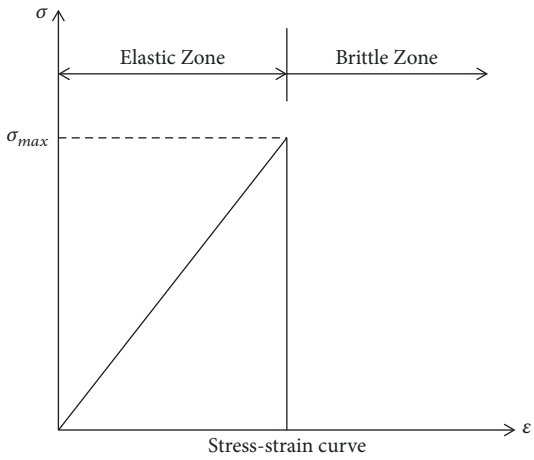

Figure 1: Linear elastic brittle law.

The discrete conservation equations of General Particle Dynamics (GPD) are expressed as

$$\frac{d\rho_i}{dt} = \sum_{j\in U} m_j v_{ij}^{\beta} W_{ij,\beta} + f \cdot \sum_{j\in D} m_j v_{ij}^{\beta} W_{ij,\beta} \tag{6}$$

$$\frac{dv_i^{\alpha}}{dt} = -\sum_{j\in U} m_j \left(\frac{\sigma_i^{\alpha\beta}}{\rho_i^2} + \frac{\sigma_j^{\alpha\beta}}{\rho_j^2} + \Pi_{ij} \right) W_{ij,\beta} - f \cdot \sum_{j\in D} m_j \left(\frac{\sigma_i^{\alpha\beta}}{\rho_i^2} + \frac{\sigma_j^{\alpha\beta}}{\rho_j^2} + \Pi_{ij} \right) W_{ij,\beta} \tag{7}$$

$$\frac{de_i}{dt} = \frac{1}{2} \sum_{j\in U} m_j v_{ij}^{\alpha} \left(\frac{\sigma_i^{\alpha\beta}}{\rho_i^2} + \frac{\sigma_j^{\alpha\beta}}{\rho_j^2} + \Pi_{ij} \right) W_{ij,\beta} + \frac{f}{2} \cdot \sum_{j\in D} m_j v_{ij}^{\alpha} \left(\frac{\sigma_i^{\alpha\beta}}{\rho_i^2} + \frac{\sigma_j^{\alpha\beta}}{\rho_j^2} + \Pi_{ij} \right) W_{ij,\beta} \tag{8}$$

where $v_{ij}^{\alpha} = v_i^{\alpha} - v_j^{\alpha}$, e_i denotes the specific internal energy of the i-th particle, x^{α}, v^{α}, and $\sigma^{\alpha\beta}$ are, respectively, elements of the spatial coordinate (X), velocity vector (V), and Cauchy stress tensor (σ) with tension taken as positive one, Π_{ij} is the artificial viscosity term used in order to stabilize computation in the presence of shock, and d/dt is the time derivative taken in the moving Lagrangian framework.

Once damage is initiated from one particle, their interactions will no longer be the same as that in the undamaged material. Although the damaged particles do not disappear and are still in the influence domain of others, the damaged particle is traction-free and the damaged particle has no influence on the surrounding particles in the stress calculation because the interaction factor f is 0, as shown in (6)-(8). For the damaged particles, since its stresses become zero, the surrounding living particles have no influence on them. A new boundary is formed, as shown in Figure 2.

3. Numerical Simulation of GPD3D on Rock Fragmentation by TBM Disc Cutters

The intrusion into rocks by one disc cutter and rock chipping formation by two disc cutters is the classical models to study the rock fragmentation by TBM cutters. In this section, models of rock fragmentation by one disc cutter and two disc cutters are established using GPD3D.

3.1. Modelling of Rock Fragmentation by One TBM Disc Cutter. As shown in Figure 3, the process of rock fragmentation by one disc cutter is three-dimensional and dynamic problem. The forces of disc cutter which are applied on the rock masses include the normal force, side force, and rolling force. Actually, rock fragmentation by TBM disc cutter is simplified as an indentation-type process [16], in which only the normal force is considered. The indentation tests have become one of the most commonly used methods to investigate the process of rock fragmentation by TBM cutters. In Figure 3, the mechanism of rock fragmentation by a disc cutter is revealed, in which the pattern of rock fragmentation by a disc cutter consists of a crushed zone and a cracked zone. The crushed zone is a highly fractured zone, and the process of indentation into rock starts with the development of a crushed zone. The crushed zone transfers the cutting forces to the body of the rock and then leads to a cracked zone. In cracked zone, there exist two major cracks, in which the cracks propagating along loading direction are called median cracks, and the other cracks propagating along lateral direction are called radial cracks.

In this section, a three-dimensional numerical model of rock fragmentation is established using GPD3D, as shown in Figure 4. Considering computational speed and mathematical precision of the numerical simulation, particle spacing is 1mm, the dimension of the numerical model is 60mm×60mm×30mm, and $60 \times 60 \times 30 = 108000$ particles represent the sample geometry in scale. Disc cutter is modelled by the normal force applied on the upper boundary through contact thickness of 15mm. In the numerical model, the rolling and side forces are neglected. The normal force is loaded in a displacement-controlled manner. During the process of rock fragmentation, the loading velocity downward remains constant at a rate of 1cm/s. A time step of 10^{-6}s is adopted to ensure the stability and efficiency of the numerical simulation, and it takes 400 steps to load the rock sample to complete the intrusion into rocks by one cutter. The lateral and bottom boundaries are regarded as fixed displacement boundaries.

In the numerical model, the parameters of coarse grained granite found in Beishan, Gansu Province, are used, because the granite has been used by Yin et al. [17] in indentation tests in which rock fragmentation under the different confining stress was studied. The properties of coarse grained granite are listed in Table 1. In the Hoek-Brown criterion, strength parameters m and s are taken as 25.0 and 1.0, respectively.

The process of rock fragmentation by one disc cutter is plotted in Figures 5(a)–5(d). In Figures 5(a)–5(d), the undamaged particles is marked with type 2 pictured here in blue, and the damaged particles are marked with type

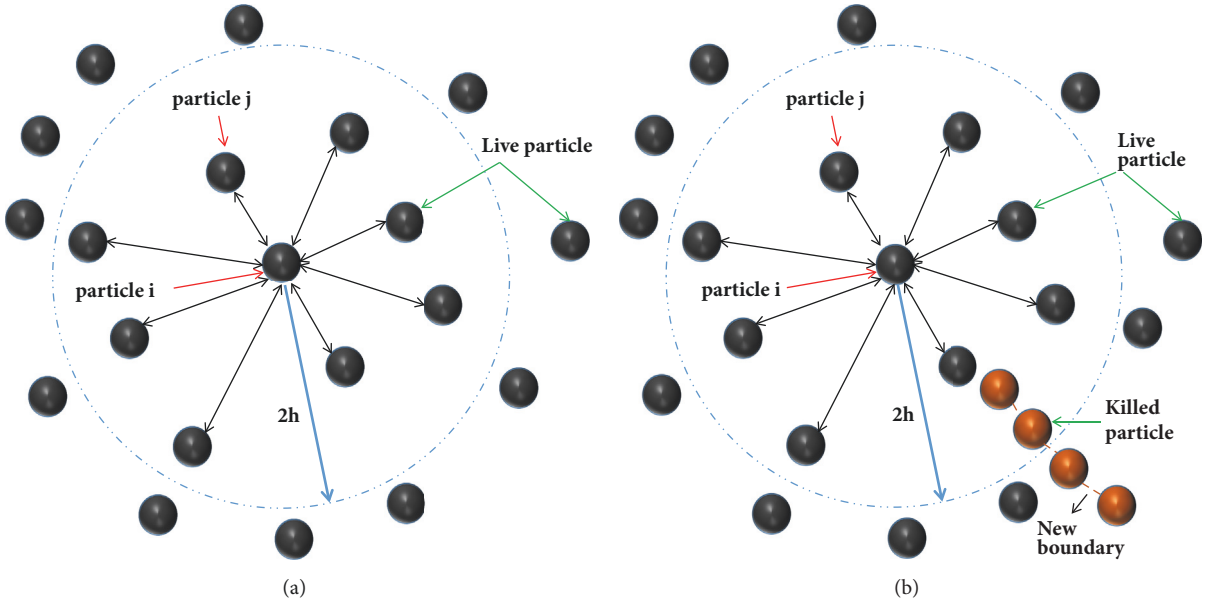

Figure 2: 3D particle discretization: (a) undamaged configuration and (b) cracked configuration.

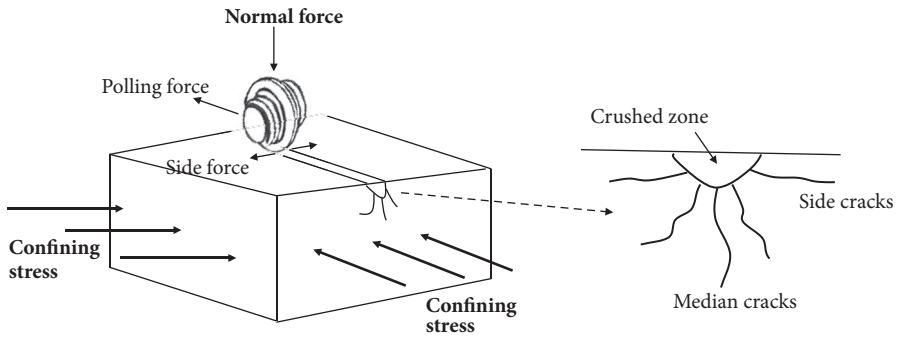

Figure 3: Mechanism of rock fragmentation by one disc cutter.

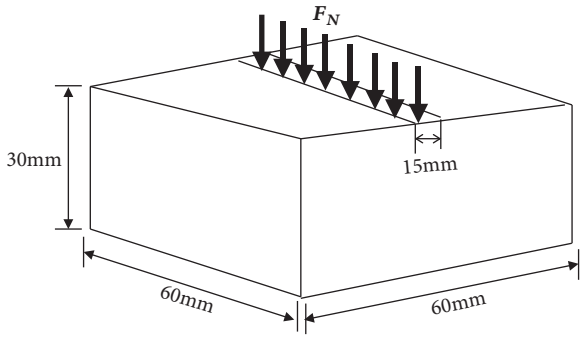

Figure 4: The 3D numerical model of rock fragmentation by one disc cutter.

3 pictured here in red. The pattern of rock fragmentation by a disc cutter consists of a crushed zone and a cracked zone [18]. When the normal force acts upon the rock mass, a crushed zone located directly under the cutter occurs, and the crushed zone is highly fractured one formed at the beginning of indentation process, as shown in Figure 5(a).

Table 1: Mechanical parameters of intact granite.

Property	value
Bulk density (kg/m^3)	2780
Elastic modulus (GPa)	23
Poisson's ratio	0.19
Uniaxial compressive strength (MPa)	108

The crushed zone contains failure zones which are induced by compressive stress and tensile stress. In the crushed zone, the spacing between neighboring particles decreases, which suggests a compressive failure mode in this zone and there are many microcracks in the failure zone comminuting the rock to powder or extremely smaller particles. At the edge of the crushed zone, there are some particles which are induced by the tensile stress and as the penetration increases, cracks are initiated from these tensile particles. Besides, the crushed zone is symmetric and there is an obvious intact rock zone because of the high confining stress which is called hydrostatic compression state [19]. It is the intact rock that

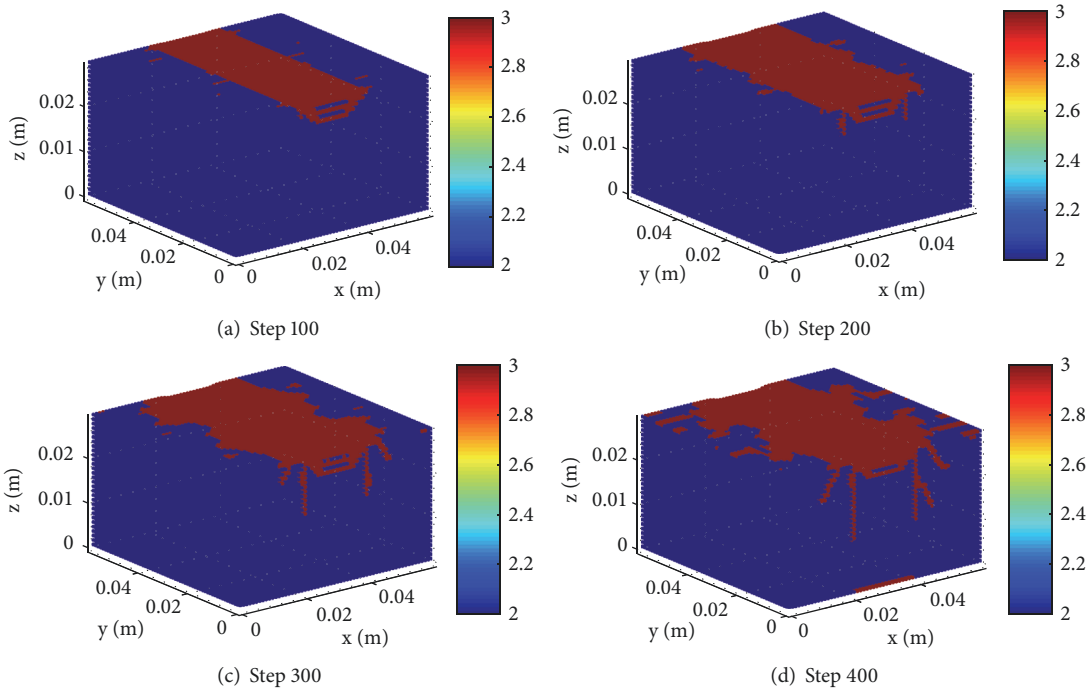

Figure 5: Process of rock fragmentation by one TBM disc cutter.

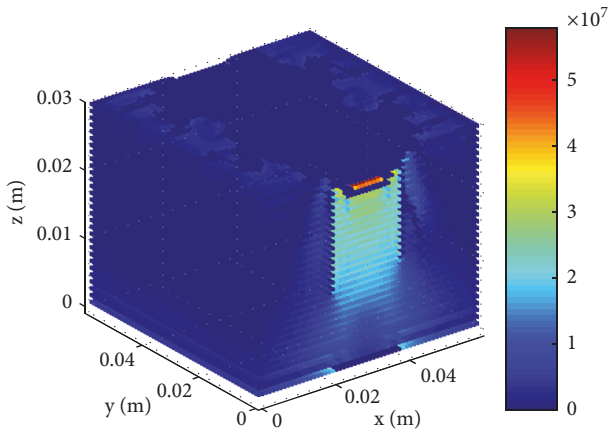

Figure 6: Principal stress contour by one disc cutter.

transfers the cutting forces to the body of the rock and then leads to a cracked zone.

As the penetration increases, cracked zone is initiated from the edge of the crushed zone, as shown in Figure 5(b). In the cracked zone, there exist major cracks defined by Pang and Goldsmith [18], which are longer than 2mm extending outward. In Figure 5(b), there exist two major cracks propagating along loading direction, which are called median cracks. The other lateral cracks are called radial cracks. The median and radial cracks, which are initiated from the tensile failure zone, propagate along the direction of the maximum principal stress.

As the penetration continuously increases, the crushed zone keeps constant, while the median and radial cracks continue to propagate along the direction of the maximum principal stress, as shown in Figures 5(c) and 5(d).

As shown in Figure 6, the stress field induced by a disc cutter is symmetrical. At first, in the crushed zone, the stress at most of particles is zero. That is related to the constitutive model adopted in this paper; an elastic brittle law is applied to analyze every particle, and it is assumed that one particle is killed when its stresses satisfy the critical value; then the stress is reduced to zero at the killed particle, while, in the obvious intact rock within the crushed zone, the particles are not damaged and the stress is high. Just as the existence of high stress, the intact rock within the crushed zone can transfer the cutting forces to the body of the rock. Moreover, beneath the crushed zone, there is a high stressed column, whose width seems to be equal to the contact width. Due to the elastic brittle law, during the propagation of median cracks, the stress at the position of median cracks is reduced to zero, and stress redistribution occurs; then a high stressed zone appears

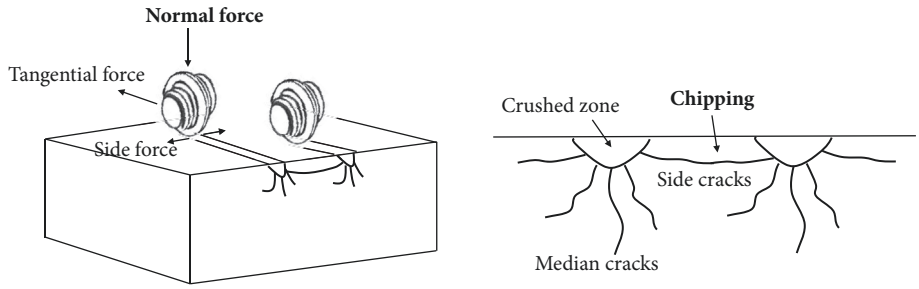

Figure 7: Mechanism of rock fragmentation by two TBM disc cutters.

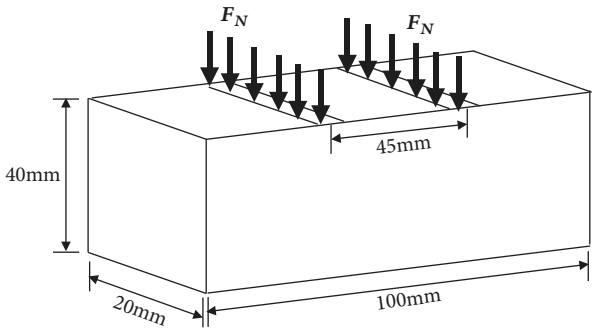

Figure 8: The 3D numerical model of rock fragmentation by two TBM disc cutters.

beneath the crushed zone with an increase in cutter loading. In addition, the stresses are extremely high at location close to the loading point and decrease with increasing the distance away from the loading point, as shown in Figure 6.

3.2. Modelling of Rock Fragmentation by Two Disc Cutters. As shown in Figure 7, the mechanism of rock fragmentation by two disc cutters is described, and chippings are formed when the side cracks between two cutters coalesce with each other. In Figure 8, the GPD3D model with two disc cutters is established. The dimension of the numerical model is 100mm×20mm×40mm, and the center distance between two cutters is 45mm. The properties of rock material, loading, and boundary conditions in the numerical model of two disc cutters are the same as that in the numerical model of one disc cutter.

The process of rock fragmentation by two disc cutters is plotted in Figures 9(a)–9(d). In the initial stage, each cutter independently acts on the rock and the crushed zones occur, as shown in Figure 9(a). Because of the interaction of two cutters, the propagation direction of the side cracks between two cutters is changed and many damage points occur near surface, as shown in Figures 9(b) and 9(c). As the penetration continuously increases, the damage points between two cutters coalesce with each other, and the chippings are formed, as shown in Figure 9(d). Figure 9(e) shows the crushed zone and crack distribution under two disc cutters in cross section at y=0.01m.

The stress fields induced by two disc cutters in cross section at y=0.01m are plotted in Figure 10. The stress fields beneath each disc cutter induced by two disc cutters are similar to those induced by one disc cutter. In the crushed zones, the stress at most of particles is zero, and in the obvious intact rock within the crushed zone, the stress is very high. The largest value of stress appears in the side of the crushed zones. Beneath each crushed zone, there is a high stressed column, whose width seems to be equal to the contact width, and the stress gradually decreases with increasing the distance away from the crushed zone. Besides, the stress at the rock chips close to the free surface is zero, and the stress beneath these chips is comparatively high.

4. Validation of the GPD3D to Model Rock Fragmentation under Different Confining Stress

In order to demonstrate the effectiveness of GPD3D on rock fragmentation by TBM cutter, in this section, the intrusion into rocks by one disc cutter under different confining stress is simulated using GPD3D and the results are compared with experimental data.

4.1. Modelling of Rock Fragmentation under Different Confining Stress. In the deep tunnels, stress is one of the most important factors affecting the process of TBM tunneling excavation. The stress state near the tunnel face can be defined as a biaxial stress one, as shown in Figure 11(a). In Figure 11(b), the GPD3D numerical model based on the biaxial stress state is set up, and the confining stress perpendicular to the cutting trace of cutter is labeled by σ_1 and the confining stress parallel to the cutting trace of cutter is labeled by σ_2. The properties of rock material, dimension, loading, and boundary conditions in the present numerical model are the same as those in the numerical model in Section 3.1.

In order to demonstrate the effectiveness of GPD3D on rock fragmentation by TBM cutter, the different confining stresses exerting on the rock are listed in Table 2, which are based on the tests of Yin et al. [4]. From Table 2, the maximum confining stress varies from 5MPa to 25MPa, while the minimum confining stress keeps constant, which is equal to 5MPa. Besides, in the GPD3D numerical simulation, the corresponding penetration depth under the different confining stress is adopted based on the indentation tests.

4.2. Numerical Results of Rock Fragmentation under the Minimum Confining Stress of 5MPa. The patterns of rock fragmentation under the minimum confining stress of 5MPa

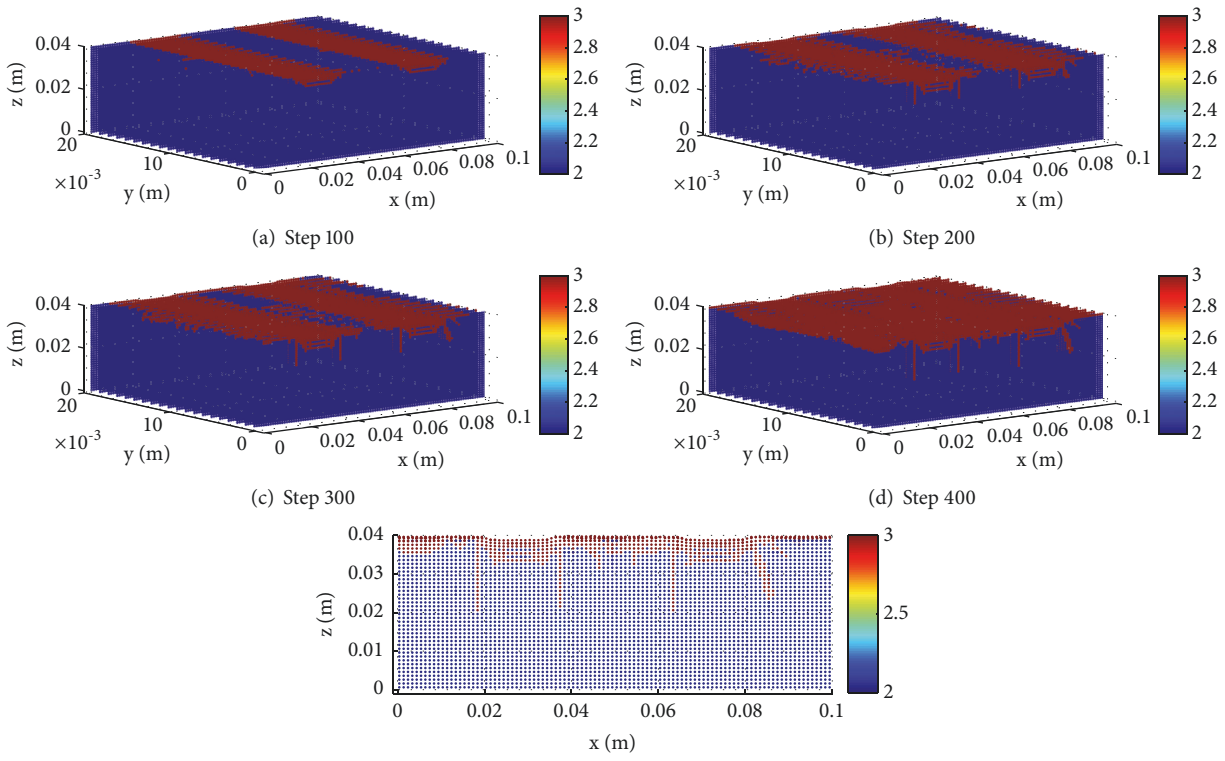

Figure 9: Process of rock fragmentation by two TBM disc cutters.

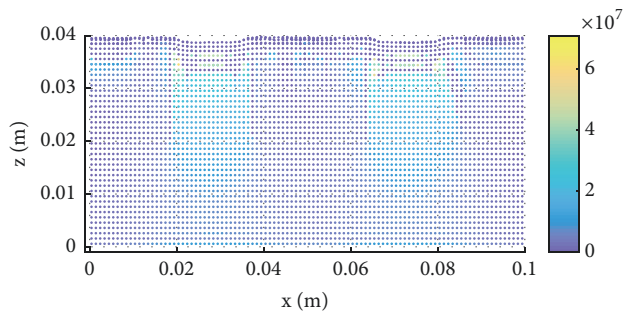

Figure 10: Principal stress contour by two TBM disc cutters.

Table 2: The different confining conditions.

σ_2(MPa)			5		
σ_1(MPa)	5	10	15	20	25

are displayed in Figures 12(a)–12(e), in which the biaxial stress state is denoted by σ_2/σ_1. In order to directly observe the crushed zone and cracks distribution under the different confining stress, cross section at y=0.01m is analyzed. Here, the crack initiation force F_{cd} and crack angle defined by Yin et al. are introduced. The crack initiation force F_{cd} is the force for crack initiation at the beginning point of unstable growth of cracks and the crack angle is defined as the angle between the lateral cracks and free surface, as shown in Figures 12(a)–12(e).

Compared with the numerical model without confining stress, median cracks do not occur in the numerical sample under the confining conditions [6]. It is consistent with the previous laboratory tests and numerical results under the confining conditions, in which vertical fracture is restrained and cracks tend to propagate towards the free edges. From Figures 12(a)–12(e), the maximum crack angle decreases, while the size of crushed zone slightly varies with increasing the confining stress σ_1.

In order to investigate the effects of the confining stress on rock fragmentation, the concrete numerical data are listed in Table 3. It is found from Table 3 that the maximum crack angle gradually decreases with increasing the confining stress σ_1 when the confining stress σ_2 is equal to 5MPa; the maximum crack angle decreases from 55° to 37° with the maximum confining stress σ_1 varying from 5MPa to 25MPa when σ_2 is

Table 3: The numerical results under the minimum confining stress of 5MPa.

The confining stress levels σ_2/σ_1	The crack initiation force F_{cd} (KN)	The maximum crack angle (^{0})
5/5	31	55
5/10	40.8	45
5/15	48.8	40
5/20	59	38
5/25	64.4	37

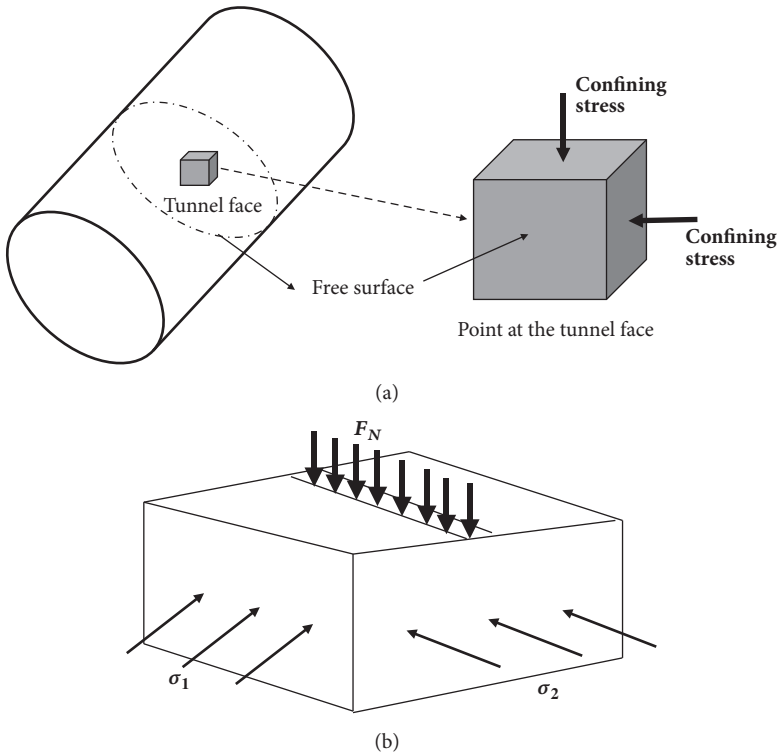

Figure 11: Stress state near the tunnel face and the 3D numerical model under different confining stress.

equal to 5MPa. That is to say, the cracks induced by one cutter tend to propagate towards the free surface with increasing σ_1. The extension of the cracks towards the free surface obtained from the proposed method is consistent with the previous experimental and numerical results obtained by Huang et al. [2].

It is found from Table 3 that the value of F_{cd} increases from 31KN to 64.4KN with σ_1 increasing from 5MPa to 25MPa when σ_2 is equal to 5MPa. It is implied from Table 3 that thrust for TBM performance under higher confining stress is higher than that under lower confining stress. The present numerical results are consistent with the observed data from TBM tunneling, in which the disk consumption for a tunnel excavation under high overburden is higher than that under lower overburden [3].

4.3. Comparisons with Experimental Results. The comparisons of the numerical and experimental results conducted by Yin et al. (2014) in Figures 13(a)–13(e) are displayed in Figures 14(a) and 14(b). It is found from Figures 12 and 13 that the numerical results of rock fragmentation under the different confining stress are in good agreement with the experimental data by Yin et al. [4]. It is also observed that the maximum crack angle obtained from the proposed method well agrees with that obtained from the experimental observations, as shown in Figure 14(a). To compare the numerical results with the indentation test in the same size, the crack initiation forces in the numerical sample are determined from the geometric similarity ratio. It is found that there is little relative error between the numerical results and experimental data when the ratio of the minimum confining stress to the maximum confining stress is equal to 5/5MPa, and the relative error between the numerical results and experimental results increases with decreasing the ratio of the minimum confining stress to the maximum confining stress.

5. The Effects of Equivalent Confining Stress on Rock Fragmentation by One TBM Disc Cutter

5.1. Modelling of Rock Fragmentation under the Equivalent Confining Stress. In this section, the GPD3D is used to

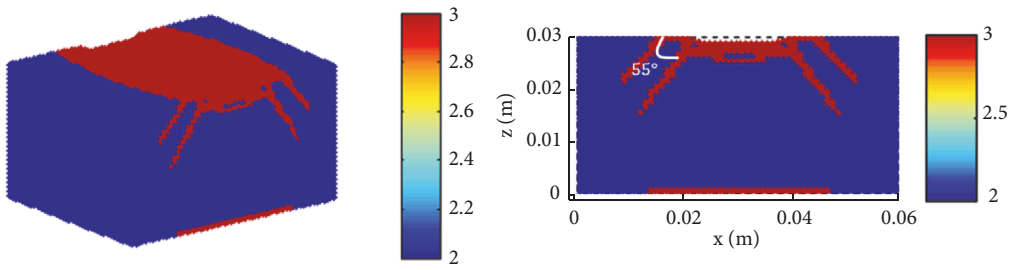

(a) 5/5MPa

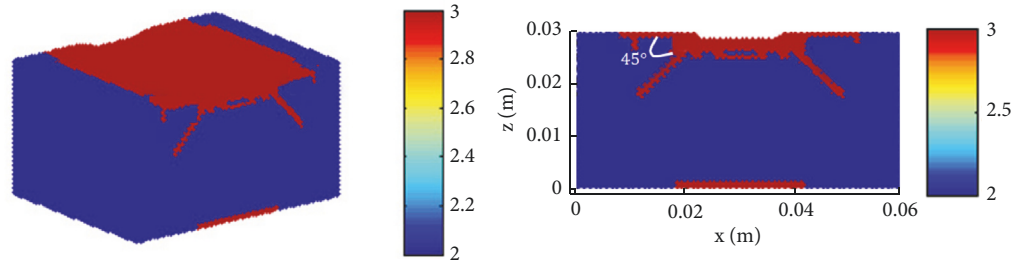

(b) 5/10MPa

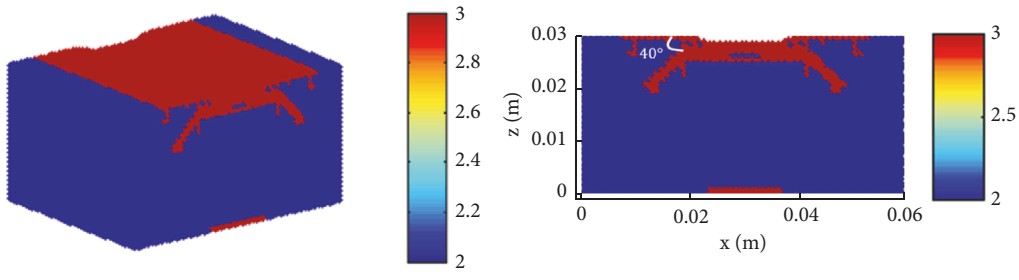

(c) 5/15MPa

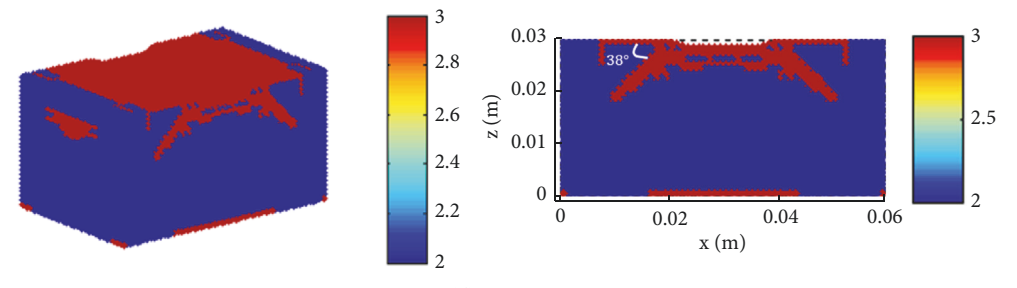

(d) 5/20MPa

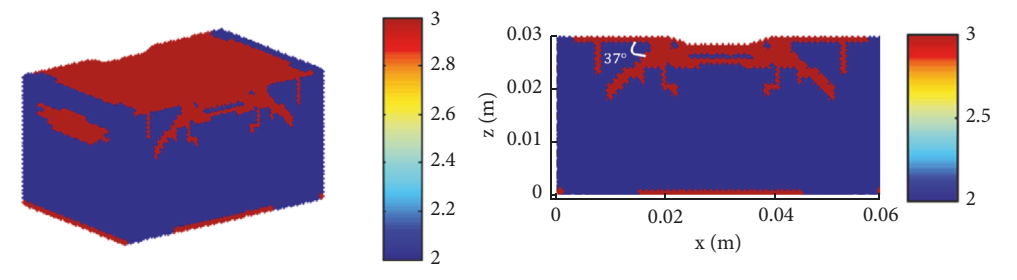

(e) 5/25MPa

Figure 12: The pattern of rock fragmentation under the minimum confining stress of 5MPa.

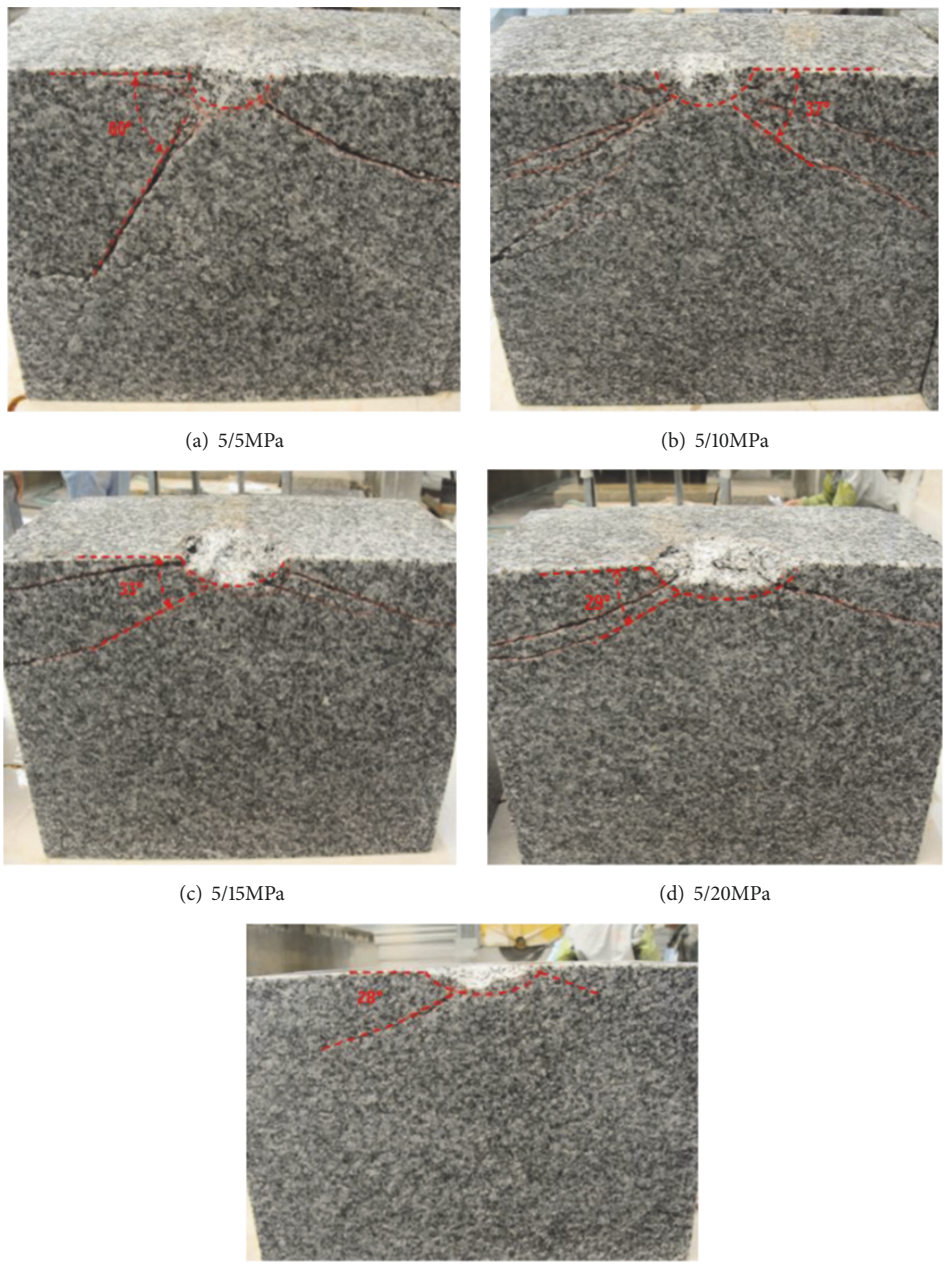

(a) 5/5MPa (b) 5/10MPa

(c) 5/15MPa (d) 5/20MPa

(e) 5/25MPa

Figure 13: The experimental results of distribution of cracks in granite samples with the minimum confining stress of 5Mpa [4].

Table 4: The equivalent confining conditions.

σ_2(MPa)	5	10	15	20	25
σ_1(MPa)	5	10	15	20	25

research the effects of equivalent confining stress on rock fragmentation by one TBM disc cutter. The numerical model is the same as that in Figure 11(b), and the properties of rock material, dimension, loading, and boundary conditions in the present numerical model are the same as those in the numerical model of Section 4.1. The equivalent confining stresses exerting on the rock are listed in Table 4.

5.2. Numerical Results of Rock Fragmentation under the Equivalent Confining Stress. The patterns of rock fragmentation under the equivalent confining stress are plotted in Figures 15(a)–15(e), and cross section at y=0.01m is analyzed. The size of crushed zone is an important factor reflecting the cutting efficiency. The formation of the crushed zone generates energy dissipation. Therefore, the smaller the crushed zone, the higher the cutting efficiency from energy dissipation point of view. The size of crushed zone almost keeps constant when the equivalent confining stress is equal to 5MPa and 10MPa, while it dramatically decreases when the equivalent confining stress varies from 10MPa to 15MPa; then it keeps

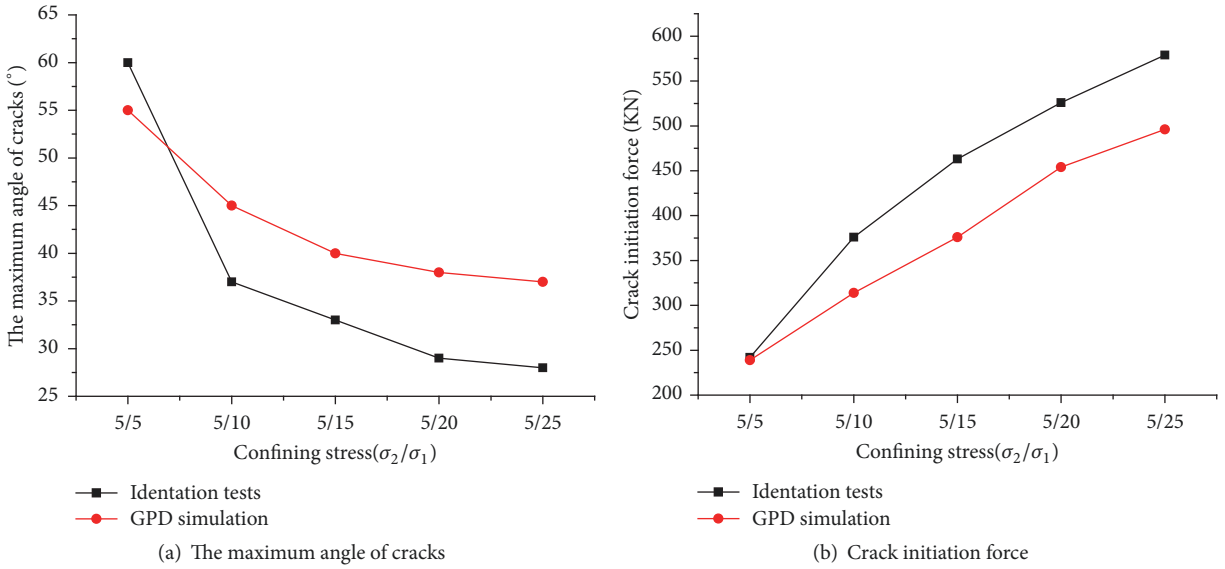

(a) The maximum angle of cracks

(b) Crack initiation force

Figure 14: The comparison of the numerical and experimental results under the minimum confining stress of 5MPa.

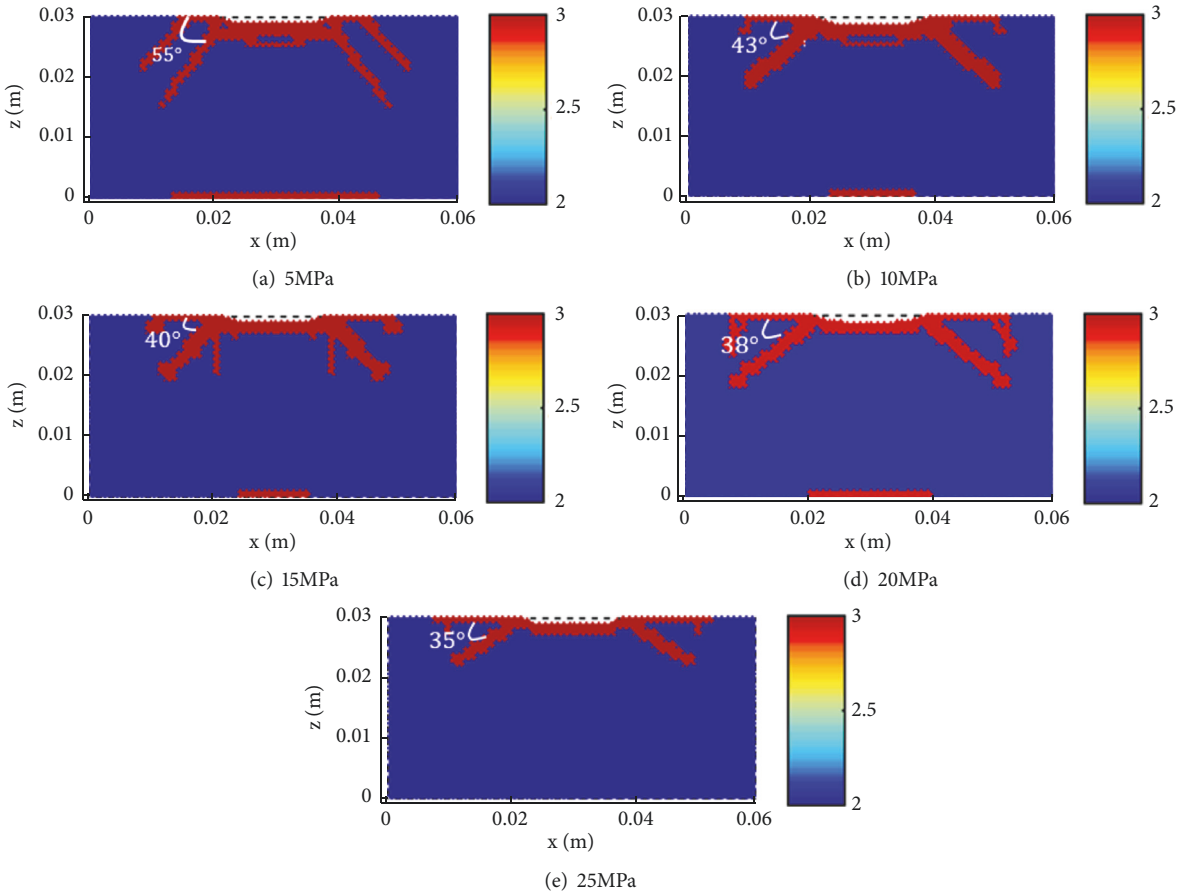

(a) 5MPa

(b) 10MPa

(c) 15MPa

(d) 20MPa

(e) 25MPa

Figure 15: The pattern of rock fragmentation under the equivalent confining stress.

Table 5: The numerical results under the equivalent confining stress.

The equivalent confining stress (MPa)	The crack initiation force F_{cd} (KN)	The maximum crack angle (°)
5	31	55
10	49.2	43
15	63	40
20	76	38
25	109	35

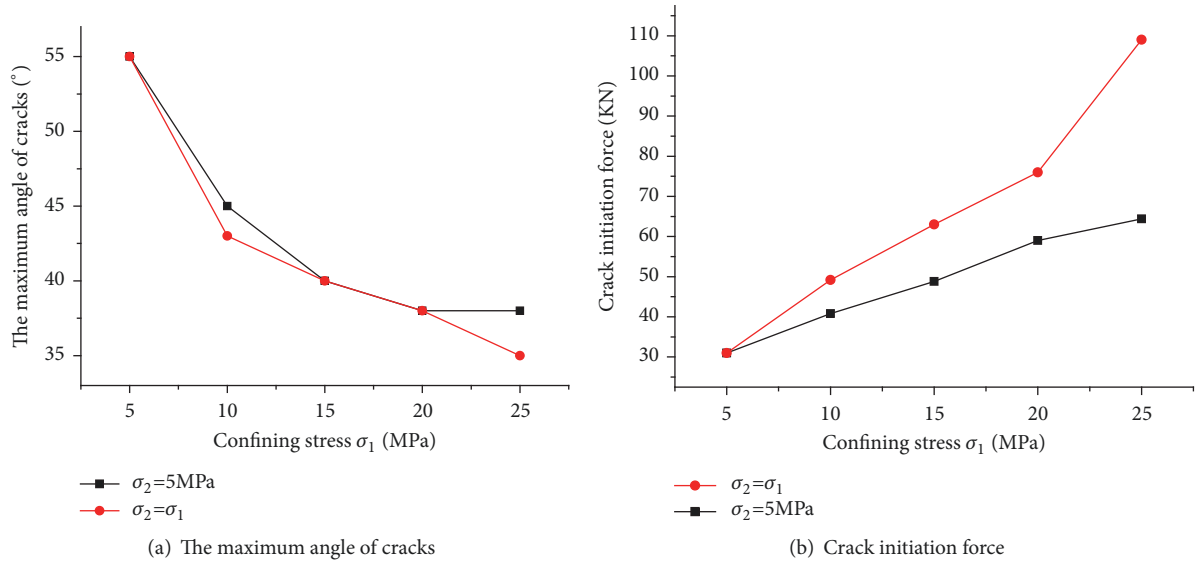

(a) The maximum angle of cracks

(b) Crack initiation force

Figure 16: The comparison of the numerical results under two different confining stress conditions.

constant when the equivalent confining stress varies from 15MPa to 25MPa. It is implied that rock fragmentation becomes easier when the equivalent confining stress is equal to 15MPa.

The concrete numerical data under the equivalent confining stress condition are listed in Table 5. It is found from Table 5 that the value of F_{cd} increases from 31KN to 109KN when the equivalent confining stress increases from 5MPa to 25MPa. It is indicated that the thrust for TBM performance under the higher stress confinement is higher than that under the lower stress confinement. It is also observed from Table 5 that the maximum crack angle obviously decreases from 55° to 43° when the equivalent confining stress increases from 5MPa to 10MPa, while the maximum crack angle gradually decreases from 43° to 35° when the equivalent confining stress increases from 10MPa to 25MPa.

The comparisons of the numerical results under different confining conditions are plotted in Figures 16(a) and 16(b). In Figure 16, the red line represents the equivalent confining stress, and the black line represents the minimum confining stress of 5MPa with the various maximum confining stress. It is found from Figure 16(a) that the maximum crack angle under two different confining conditions decreases, and the difference of the maximum crack angle under two different confining conditions is very little. It is observed from Figure 16(b) that the crack initiation forces increase under two different confining conditions with increasing the confining stress σ_1, and the crack initiation forces increase faster under the equivalent confining stress than that under the minimum confining stress of 5MPa with the various maximum confining stress.

6. Conclusions

A three-dimensional numerical method known as General Particle Dynamics (GPD3D) is developed to simulate rock fragmentation by TBM disc cutters. The 3D Hoek-Brown criterion is applied to determine damage initiation. Damage is initiated from one particle when stresses in the particle satisfy the failure criterion. The rock fragmentation by one disc cutter and two disc cutters is investigated using GPD3D. The mechanism of rock fragmentation is demonstrated. The present numerical results on the crushed zone, initiation and propagation of cracks, and the chipping of rocks agree well with experimental observations and numerical results.

The effects of different confining stress on rock fragmentation, in which the minimum confining stress is 5MPa and the maximum confining stress ranged from 5MPa to 25MPa, are investigated using GPD3D. Comparing the numerical results with the indention tests, the effectiveness of GPD3D on rock fragmentation by one TBM disc cutter under different confining stress is validated.

Moreover, the effects of equivalent confining stress on crack initiation force and the maximum angle of cracks

are also studied using GPD3D. It is found that, from the numerical results, rock fragmentation becomes easier when the equivalent confining stress is equal to 15MPa from energy dissipation point of view.

Comparing two different confining conditions, it is found that the crack initiation forces significantly increase as the confining stress increases, while the maximum angle of cracks decreases as the confining stress increases. The difference of the maximum crack angle under two different confining conditions can be negligible, while the crack initiation forces increase faster under the equivalent confining stress than that under the minimum confining stress of 5MPa with the various maximum confining stress.

Data Availability

The data used to support the findings of this study are available from the corresponding author upon request.

Conflicts of Interest

The authors declare that there are no conflicts of interest regarding the publication of this paper.

Acknowledgments

This work was supported by National program on Key Basic Research project (973 Program) (Grant no. 2014CB046903), the Doctoral Scientific Research Foundation and the Youth Support Programme of Henan University of Technology (nos. 2018BS005 and 2018QNJH27), and Key Research Projects of Institution of Higher Learning in Henan Province (no. 18A440011).

References

[1] K. Gehring, "Design criteria for TBMs with respect to real rock pressure," in *Proceedings of the Tunnel Boring Machines: Trends in Design and Construction of Mechanized Tunneling*, pp. 43–53, Hagenberg, Austria, 1995.

[2] H. Huang, B. Damjanac, and E. Detournay, "Normal wedge indentation in rocks with lateral confinement," *Rock Mechanics and Rock Engineering*, vol. 31, no. 2, pp. 81–94, 1998.

[3] N. Innaurato, C. Oggeri, P. P. Oreste, and R. Vinai, "Experimental and numerical studies on rock breaking with TBM tools under high stress confinement," *Rock Mechanics and Rock Engineering*, vol. 40, no. 5, pp. 429–451, 2007.

[4] L. J. Yin, Q. M. Gong, H. S. Ma, J. Zhao, and X. B. Zhao, "Use of indentation tests to study the influence of confining stress on rock fragmentation by a TBM cutter," *International Journal of Rock Mechanics and Mining Sciences*, vol. 72, pp. 261–276, 2014.

[5] Q.-M. Gong, J. Zhao, and Y.-Y. Jiao, "Numerical modeling of the effects of joint orientation on rock fragmentation by TBM cutters," *Tunnelling and Underground Space Technology*, vol. 20, no. 2, pp. 183–191, 2005.

[6] H. Ma, L. Yin, and H. Ji, "Numerical study of the effect of confining stress on rock fragmentation by TBM cutters," *International Journal of Rock Mechanics and Mining Sciences*, vol. 48, no. 6, pp. 1021–1033, 2011.

[7] J. Liu, P. Cao, and K. Li, "A Study on Isotropic Rock Breaking with TBM Cutters Under Different Confining Stresses," *Geotechnical and Geological Engineering*, vol. 33, no. 6, pp. 1379–1394, 2015.

[8] P. O. Bouchard, F. Bay, Y. Chastel, and I. Tovena, "Crack propagation modelling using an advanced remeshing technique," *Computer Methods Applied Mechanics and Engineering*, vol. 189, no. 3, pp. 723–742, 2000.

[9] F. Donze, V. Richefeu, and S. Magnier, "Advances in discrete element method applied to soil rock and concrete mechanics," *Electronic Journal of Geological Engineering*, vol. 8, pp. 1–44, 2009.

[10] J. Bi, X. P. Zhou, and Q. H. Qian, "The 3D numerical simulation for the propagation process of multiple pre-existing flaws in rock-like materials subjected to biaxial compressive loads," *Rock Mechanics and Rock Engineering*, vol. 49, no. 5, pp. 1611–1627, 2016.

[11] X. P. Zhou, J. Bi, and Q. H. Qian, "Numerical simulation of crack growth and coalescence in rock-like materials containing multiple pre-existing flaws," *Rock Mechanics and Rock Engineering*, vol. 48, no. 3, pp. 1097–1114, 2015.

[12] H. Jiang, "A simple, convenient three-dimensional Hoek-Brown criterion for rocks," *Chinese Journal of Rock Mechanics and Engineering*, vol. 34, no. 1, pp. 2996–3004, 2015.

[13] E. Hoek, "Estimating Mohr-Coulomb friction and cohesion values from the Hoek-Brown failure criterion," *International Journal of Rock Mechanics and Mining Sciences & Geomechanics Abstracts*, vol. 27, no. 3, pp. 227–229, 1990.

[14] E. Hoek, "Strength of jointed rock masses," *Géotechnique*, vol. 33, no. 3, pp. 187–223, 1983.

[15] E. Hoek and E. T. Brown, "Practical estimates of rock mass strength," *International Journal of Rock Mechanics and Mining Sciences and Geomechanics Abstracts*, vol. 34, no. 8, pp. 1165–1186, 1997.

[16] M. Hood and F. Roxborough, "Report: a review of non-explosion rock breaking," Tech. Rep., HDRK Mining Research Ltd, Toronto, Canada, 1989.

[17] L. J. Yin, Q. M. Gong, and J. Zhao, "Study on rock mass boreability by TBM penetration test under different in situ stress conditions," *Tunnelling and Underground Space Technology*, vol. 43, pp. 413–425, 2014.

[18] S. S. Pang and W. Goldsmith, "Investigation of crack formation during loading of brittle rock," *Rock Mechanics and Rock Engineering*, vol. 23, no. 1, pp. 53–63, 1990.

[19] H. Y. Liu, S. Q. Kou, P.-A. Lindqvist, and C. A. Tang, "Numerical simulation of the rock fragmentation process induced by indenters," *International Journal of Rock Mechanics and Mining Sciences*, vol. 39, no. 4, pp. 491–505, 2002.